Theoretical studies of atomic vibrations on the Si(001)(2×1) surface

H. M. Tütüncü, S. J. Jenkins, and G. P. Srivastava
Physics Department, University of Exeter, Stocker Road, Exeter EX4 4QL, United Kingdom
(Received 10 September 1996; revised manuscript received 10 April 1997)

We present adiabatic bond-charge model studies of surface-phonon modes on the symmetric and asymmetric dimer models of the Si(001)(2×1) surface. The structural and electronic information necessary for these calculations is obtained using the *ab initio* pseudopotential method. We find that dimerization leads to the formation of new peaks in the phonon density of states. In particular, the peak in the stomach gap at around 30 meV is a strong signature of dimer formation. [S0163-1829(97)08931-5]

I. INTRODUCTION

The Si(001)(2×1) surface has been among the most widely studied of semiconductor surfaces because of its importance to device physics. Over the past two decades, most experimental and theoretical works have been devoted to the determination of surface atomic geometry and surface electronic states. Structural studies using low energy electron diffraction,[1–3] reflection high energy electron diffraction,[4] x-rays,[5–7] and He atoms[8] indicate an asymmetric dimer geometry for the top surface layer, while surface electronic bands have been mapped by photoemission.[9,10] Although the symmetric dimer geometry is supported by some older theoretical works,[11–13] recent well-converged *ab initio* pseudopotential total energy calculations favor the asymmetric dimer configuration.[14–16]

In truth, the low temperature clean Si(001) surface is now understood to reconstruct into a $c(4\times2)$ phase consisting of alternately buckled asymmetric dimers.[17] Correlated dynamic flipping of these dimers can lead to room temperature scanning tunneling microscopy detecting only a (2×1) periodicity.[18] Computational practicalities have thus far restricted theoretical calculations of the $c(4\times2)$ phase to a small number of structural / electronic,[18–20] and lattice dynamical[15,18,29] studies. Nevertheless, the study of the (2×1) reconstructed surface is expected to reveal similar underlying physics to the $c(4\times2)$ phase, since both are composed of the same asymmetric dimer building blocks. Investigation of the Si(001)(2×1) surface is thus a vital first step towards a thorough understanding of the $c(4\times2)$ reconstructed surface.

While He-atom-scattering[21,22] and high-resolution electron energy-loss spectroscopy[23,24] have been used to study surface-phonon modes of some III-V(110) surfaces, only one experimental work (Brillouin light scattering[25]) has been done on the surface phonons of Si(001)(2×1). On the theoretical side, Allan and Mele[26] presented the first study of the surface-phonon spectrum of Si(001)(2×1) by using a tight-binding theory. The tight-binding model has since been applied to the Si(001)(2×1) surface by several groups.[27–30] Recently, Fritsch and Pavone[15] have used a linear response approach, based on the density functional perturbative scheme, to study surface phonons on this surface. One of the important points to note in their work is that the lowest phonon frequency at the $\overline{K}$ point (corner of surface Brillouin zone) has been placed at a significantly lower energy than in any of the tight-binding calculations.[26–30]

As a phenomenological theoretical scheme, the adiabatic bond-charge model (BCM) has been found to be successful in studies of phonon modes in bulk semiconductors,[31,32] on semiconductor surfaces,[33,34] as well as on the hydrogen-covered silicon surface.[35,36] In the present paper, we have used this model to study atomic vibrations at the Si(001)(2×1) surface within a repeated slab scheme. The bond-charge model represents an intermediate level of theory between tight-binding and *ab initio* calculations, in the sense that it requires far fewer parameters than the former, yet far less computer time than the latter. In view of the disagreement between existing tight-binding and *ab initio* calculations of lattice dynamics, there exists a clear need for further clarification, which our approach can supply.

First of all we present results of an *ab initio* pseudopotential calculation[16] for the relaxed atomic geometry and the corresponding electronic states. Dangling BC positions are determined from the calculated valence electron charge density for the dangling bonds. The relaxed ionic and the corresponding BC positions are used as input to our BCM calculations. We present a detailed discussion on the polarization and localization of vibrational modes along symmetry directions on the surface Brillouin zone. We also provide discussion on the effect of surface relaxation on localized phonon modes on this surface. Our results are compared with available theoretical and experimental results.

II. THEORY

A. Atomic geometry and electronic states

The atomic geometry required as input for the phonon studies was calculated within the local density approximation to the density functional theory. The electron-ion interaction was dealt with by means of the *ab initio* pseudopotential scheme,[37] employing a basis set of plane waves up to a kinetic energy cutoff of 8 Ry. The surface was modeled within a supercell containing eight layers of Si and the equivalent of four atomic layers of vacuum. One side of the Si slab was terminated with H atoms arranged in a dihydride structure for the purpose of passivating the back surface. The other side constituted the surface of interest and was left clean,

with Si dimer formation in the [110] direction. The atomic degree of freedom was relaxed using a conjugate gradient technique, with total energy and forces supplied at each iteration by solving the Kohn-Sham equation. One semirelaxed geometry was determined by constraining the dimer to be symmetric, while a second fully relaxed geometry was determined in which the dimer took its optimum asymmetric form. Our results for the asymmetric model were briefly discussed in a recent publication.[16]

B. Lattice dynamics

In the BCM lattice dynamics of semiconductor structures characterized by a large degree of covalency are studied by incorporating the effect of valence electrons in terms of bond charges (BC's). In the adiabatic BCM for tetrahedrally bonded structures the valence electron charge density is represented by massless point particles, viz. BC's, located at the maximum charge density between neighboring atoms.

For lattice dynamical studies we have modeled the Si(001)-(2×1) surface in a repeated slab scheme, similar to that used for our plane-wave pseudopotential calculations of atomic geometry and electronic states. The supercell consisted of 16 layers of Si and a vacuum region equivalent to eight atomic layers. In this case we do not passivate one surface with H, but instead use a relaxed geometry, taken from our *ab initio* pseudopotential calculations, for each side of the slab. Atoms in the top three layers on each side are placed at their relaxed positions, while deeper lying atoms are taken at their bulk positions. Bond charges were, in general, placed midway between nearest-neighbor Si ions and given charge Ze. In order to maintain overall charge neutrality within each bulk unit cell, the Si ions were given a charge of -2 Ze. However, the bond charges representing the dangling bonds of the dimer were instead positioned and charged according to the positions and magnitudes of the maxima in the partial electronic charge densities obtained for those states from the *ab initio* pseudopotential calculation. In test calculations, we have found that changing the dangling bond-charge positions by up to 10% of the ion-BC distance results in changes to phonon frequencies of substantially less than 1%.

In all, there were 32 ions within the supercell and 62 ordinary BC's. In the semirelaxed case (i.e., the symmetric dimer geometry) the three dangling-bond-related orbital lobes on each side of the slab have maxima of equal magnitude [see Fig. 2(a)], and so we assign a BC to each with a charge of 0.33 Ze. For the fully relaxed case (i.e. asymmetric dimer geometry) these orbital lobes are inequivalent [see Fig. 2(b)] and are assigned charges of 0.55 Ze, 0.35 Ze, and 0.10 Ze. In test calculations, we have found that redistributing up to 0.05 Ze between these lobes alters phonon frequencies by much less than 1%. In total, there were 100 charged particles within the supercell for the both the relaxed and the semirelaxed geometries.

Additionally, we have performed calculations for the unrelaxed geometry, in which the surface atoms are not dimerized and possess two dangling bonds each, which we represent by BC's of charge Ze/2 positioned along the tetrahedral bonding directions at the bulk BC-ion distance. Once again there are 100 charged particles within the (2×1) supercell.

TABLE I. Force-constant parameters used in the study of Si(001)(2×1) in units of e^2/V_a, where V_a is the bulk unit cell volume and r_0 is the bond length between nearest-neighbor ions.

ϕ''_{i-i}	$\phi''_{i-\mathrm{BC}}$	ϕ'_{i-i}/r_0	$\phi'_{i-\mathrm{BC(surface)}}/r_0$	β	Z^2/ε
18.63	19.41	-1.99	-0.66	8.60	0.145

We present a detailed comparison of the phonon modes for both the symmetric and asymmetric dimer configurations, and also the unrelaxed geometry.

The model includes three types of interactions.

(i) The long-range Coulomb interaction between all particles (i.e., ions and bond charges) is controlled by the model parameter Z^2/ε, where ε is the dielectric constant of the semiconductor. The Coulomb matrix is of dimension 300×300, corresponding to a total of 100 charged particles in the supercell:

$$C^C_{\alpha\beta=x,y,z}(\kappa\kappa'|\mathbf{q})=\frac{e^2}{V_a}\frac{Z^2}{\varepsilon}\begin{bmatrix}4C_R & -2C_T\\ -2C_T^+ & C_S\end{bmatrix},$$

where C_R, C_T, C_T^+, C_S denote the ion-ion, ion-BC, BC-ion, and BC-BC matrices, respectively, and V_a is the volume of bulk unit cell. These matrices are taken into account by an Ewald technique.[38] We find that the self term ion-ion Coulomb force constant matrices are nonzero because of broken bulk symmetry in the presence of the surface.

(ii) $\phi_{i-\mathrm{BC}}$ denotes the ion-BC central potential and ϕ_{i-i} shows nearest neighbor interaction potential between ions. In order to get the first derivative of $\phi_{i-\mathrm{BC}}$ and ϕ_{i-i}, we have imposed the equilibrium condition for the unit cell described above. From this condition, we find that the first derivative of $\phi_{i-\mathrm{BC}}$ at the surface has a negative value (see Table I), while in the bulk such a parameter is assumed to be zero.[31] The second derivatives of the potentials do not appear for this equilibrium condition and thus are taken as their bulk values, since the relative distances between ion-BC, ion-ion, and BC-BC are nearly the same as the bulk values. The central force constant matrix between two particles can then be calculated as[38]

$$\Phi_{\alpha\beta=x,y,z}(\ell\kappa;\ell'\kappa')=\frac{x_\alpha x_\beta}{r^2}\left[\phi''_{\kappa\kappa'}(r)-\frac{1}{r}\,\phi'_{\kappa\kappa'}(r)\right]+\frac{\delta_{\alpha\beta}}{r}\,\phi'_{\kappa\kappa'}(r), \tag{1}$$

where r denotes magnitude of the relative distance between particle κ in ℓth unit cell, and κ' in ℓ'th unit cell, and $\phi_{\kappa\kappa'}$ represents interparticle central potential ($\phi_{i-\mathrm{BC}}$ or ϕ_{i-i}). From the above equation, we have observed that the central force-constant matrices between top three layer atoms and BC's are very different from their bulk values, indicating clearly that a careful consideration of the ion-BC force-constant matrix is very important for a study of surface dynamics.

(iii) A bond-bending potential of the Keating form,[39] involving the BC-ion-BC angle, is considered to be controlled by the parameter B_Δ,

$$V^{(\Delta)}_{\mathrm{bb}}=\tfrac{1}{2}\,B_\Delta(\mathbf{r}_{\Delta i}\mathbf{r}_{\Delta j}+a_\Delta^2)^2/4a_\Delta^2, \tag{2}$$

where B_Δ is the Keating force constant, $\mathbf{r}_{\Delta i}$ and $\mathbf{r}_{\Delta j}$ are the position vectors between the ion of type Δ and its neighboring bond charges, and a_Δ^2 is the equilibrium value of $|\mathbf{r}_{\Delta i}\cdot\mathbf{r}_{\Delta j}|$. Although we have taken B_Δ as the same as its bulk value, the elements of the short range Keating ion-BC's matrices between the top layer atoms and their neighboring BC's become very much different from their bulk values because the angle between neighboring BC's changes considerably on the relaxed surface.

The above two-body and bond-bending potentials are used to generate the elements of the short range BCM force-constant matrices. Thus, the total short range interaction matrix can be divided into three groups, the ion-ion force constant matrix R (derived from ϕ_{i-i}), the ion-BC constant matrix T (derived from $\phi_{i-\mathrm{BC}}$ and V_{bb}^{Δ}), and the BC-BC force constant matrix S (derived from V_{bb}). The coupled dynamical equations for the ion and BC displacement vectors ($\mathbf{U}_{\mathrm{ion}}$ and $\mathbf{U}_{\mathrm{BC}}$) are

$$M_{\mathrm{ion}}\omega^2\mathbf{U}_{\mathrm{ion}}=\left(R+\frac{4Z^2}{\varepsilon}\,C_R\right)\mathbf{U}_{\mathrm{ion}}+\left(T-\frac{2Z^2}{\varepsilon}\,C_T\right)\mathbf{U}_{\mathrm{BC}}, \tag{3}$$

$$m_{\mathrm{BC}}\omega^2\mathbf{U}_{\mathrm{BC}}=\left(T^+-\frac{2Z^2}{\varepsilon}\,C_T^+\right)\mathbf{U}_{\mathrm{ion}}+\left(S+\frac{Z^2}{\varepsilon}\,C_S\right)\mathbf{U}_{\mathrm{BC}}. \tag{4}$$

In the adiabatic approximation we assume m_{BC} as zero, and thus the effective ion-ion matrix (R_{eff}) is found as

$$R_{\mathrm{eff}}=\left[R+\frac{4Z^2}{\varepsilon}\,C_R\right]-\left[T-\frac{2Z^2}{\varepsilon}\,C_T\right]\left[S+\frac{Z^2}{\varepsilon}\,C_S\right]^{-1}\times\left[T^+-\frac{2Z^2}{\varepsilon}\,C_T^+\right]. \tag{5}$$

The eigensolutions of the dynamical problem are obtained by solving the secular equation

$$\left[\frac{1}{M}\,R_{\mathrm{eff}}(\mathbf{q})-\omega^2 I\right]\mathbf{U}_{\mathrm{ion}}(\mathbf{q})=0, \tag{6}$$

where M is the ionic mass matrix.

III. RESULTS

A. Surface atomic geometry and electronic states

In Fig. 1, we show schematic side and top views of the relaxed surface geometry of the Si(001)(2×1) surface. Dimerization is considered along [110], leading to a doubled periodicity in this direction, and to the formation of dimer rows along [$\bar{1}$10]. Constraining the Si dimer to be symmetric, we obtain a dimer bond length of 2.20 Å; somewhat shorter than our theoretically calculated bulk Si-Si bond length of 2.35 Å. However, removing the constraint, we find that the asymmetric dimer geometry is energetically favorable by 0.12 eV per dimer over the symmetric dimer geometry. The asymmetric dimer is buckled by 16.1° and has a bond length of 2.25 Å.[16]

In both the symmetric and asymmetric geometries, the dangling bonds on the Si dimer atoms form a π-bonding orbital with three lobes, although in the asymmetric case

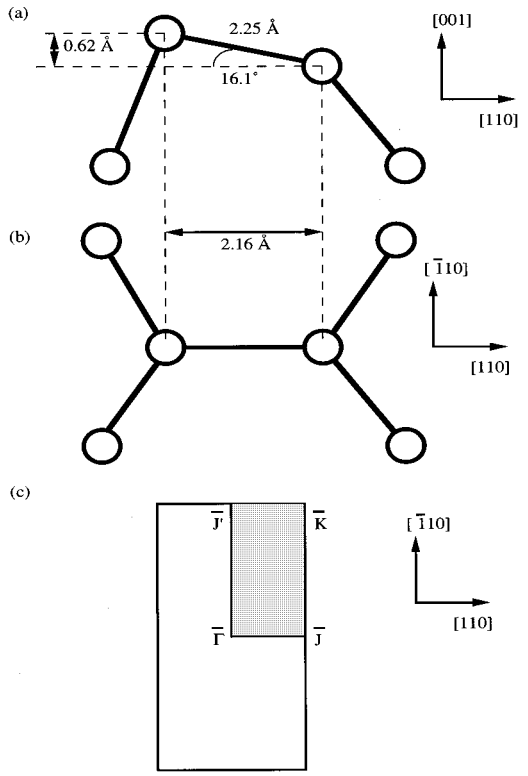

FIG. 1. Schematic (a) side and (b) top views of the asymmetric relaxed surface geometry of the Si(001)(2×1) surface. Also shown is (c) the surface Brillouin zone.

charge transfer denudes one of the outer lobes, while the other is enhanced (see Fig. 2). Three bond charges are assigned to mimic these lobes, with a total charge equivalent to two electrons. The charge and position of each individual bond charge is determined by the magnitude and position of the charge density maximum of the lobe which it mimics (see discussion in Sec. II B).

The electronic band structure of the asymmetric dimer geometry is shown in Fig. 3. The π-bonded dangling-bond orbital appears as the highest occupied surface state, just encroaching into the fundamental gap, while a π^*-antibonding orbital accounts for the lowest unoccupied surface state. Comparison with experimental results[40] is good, but not perfect. Experiment reveals two occupied surface states. The lower lying of these matches our results very well, but the higher lying band has never been reported in any previous theoretical calculation for the Si(001)(2×1) surface[40] and does not appear in ours. Such a band has, however, been noted by Northrup[20] and by Fritsch and Pavone[15] in calculations for the $c(4\times2)$ reconstructed surface.

B. Surface phonons

In Fig. 4, we have plotted the projected bulk Si phonon energies (hatched region) and the results for the asymmetric dimer geometry are shown by thick lines, while the results for the symmetric dimer geometry are shown by dashed lines. For surface phonons with wave vector along $\bar{\Gamma}$-$\bar{J}$, we find no appreciable change in the dispersion between the two models, while for those with a finite wave vector component along $\bar{\Gamma}$-$\bar{J}'$ (the dimer row direction) there is noticeable

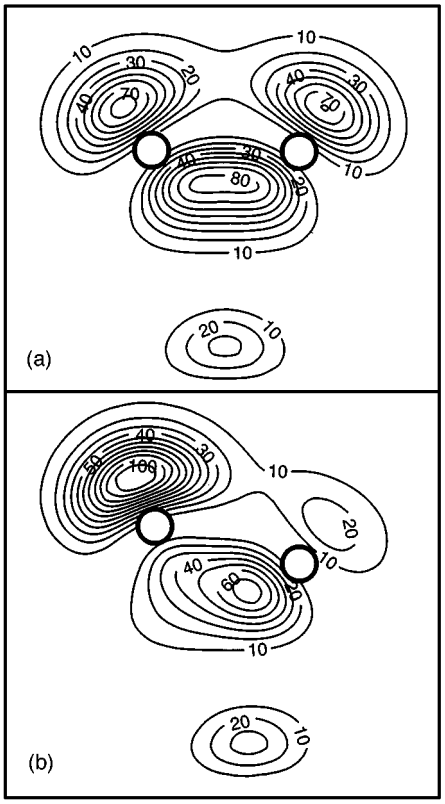

FIG. 2. Electronic charge density for the dangling bond charges on Si(001)(2×1): (a) symmetric dimer, (b) asymmetric dimer. The electron density is normalized to the number of electrons in the supercell (i.e., 68 in all the pseudopotential calculations reported here).

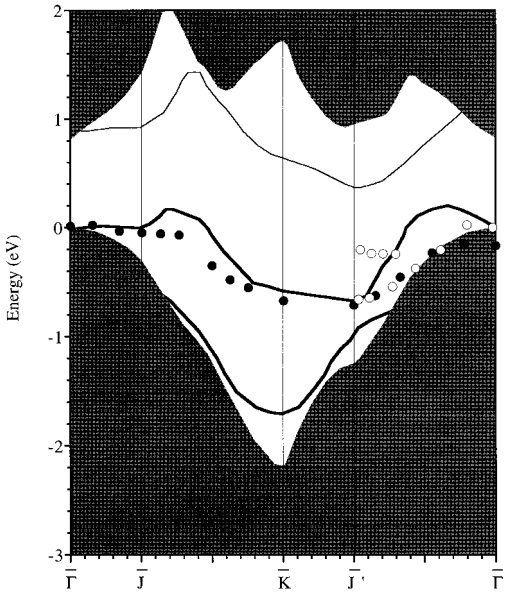

FIG. 3. Surface electronic states for the asymmetric dimer model of Si(001)(2×1). Solid lines show theoretical results, while filled circles show the experimental results of Uhrberg *et al.* (Ref. 9) and open circles show the experimental results of Johansson *et al.* (Ref. 10).

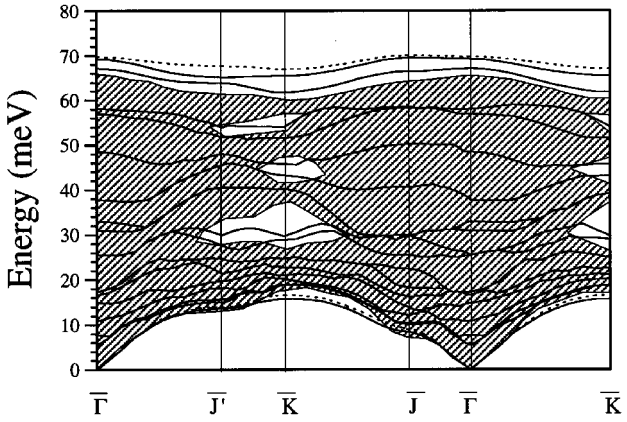

FIG. 4. The dispersion of surface-phonon modes on the Si(001)(2×1) surface. The calculated results for the asymmetric surface geometry are shown by thick solid curves. The results for the symmetric surface geometry are shown by dashed curves.

change in the dispersion. In general the tilt of the dimer results in the energy of zone-edge surface phonons dropping by up to 2 meV. We have observed that the lowest surface-phonon mode (Rayleigh branch) becomes more distinct at $\bar{K}$ from the bulk phonon modes than was the case for the symmetric dimer geometry.

We have also presented (Fig. 5) the phonon density of states of the repeated slab with the asymmetric relaxed surface geometry. For comparison, the phonon density of states for bulk Si is shown by the dashed curve. Some peaks characterized by atomic vibrations on the Si(001)(2×1) surface are labeled S_1 to S_5 in the figure. The peak S_1 at around 7 meV is due to the Rayleigh waves mainly along the $\bar{\Gamma}$-$\bar{J}$ direction, while S_2 and S_3 are peaks due to localized stomach gap phonon states. The peaks labeled S_4 and S_5 are the two surface states lying above the bulk continuum (see also Fig. 4).

(i) The effect of surface relaxation on vibrations. For the unrelaxed surface calculation we have considered the ideally terminated bulk positions for the ions, and placed bond charges of magnitude Ze/2 at their bulk positions along each of the dangling bonds from the top layer ions. In Fig. 6, we

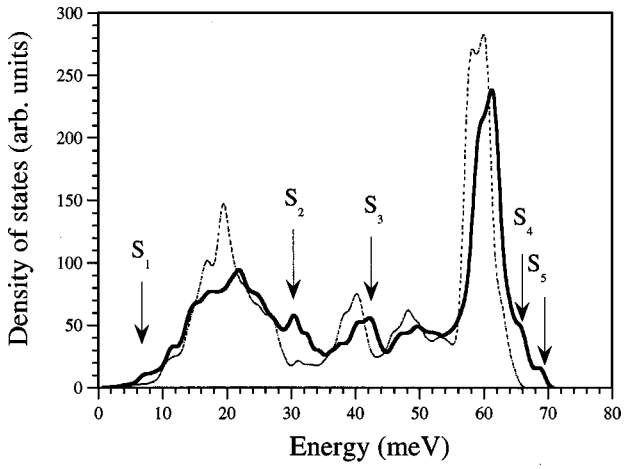

FIG. 5. The density of phonon states for the slab supercell with the asymmetric surface geometry (solid curve) is compared with the bulk density of states (dotted curve). S_1-S_5 represent surface peaks.

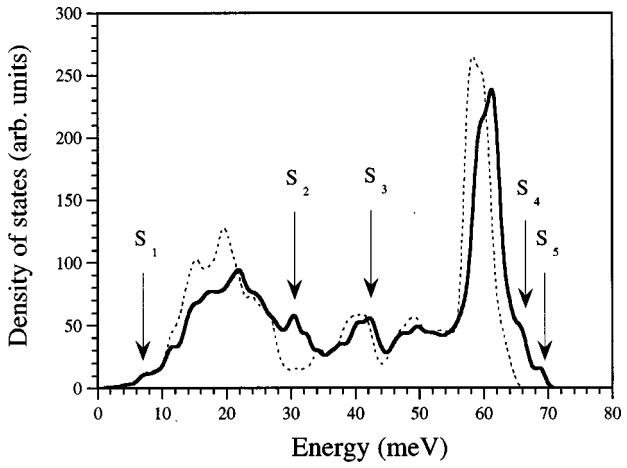

FIG. 6. The density of phonon states on Si(001). The solid curve is obtained from the (001) slab supercell calculation with the asymmetric surface geometry, while the dotted curve shows the density of states with the ideally terminated surface geometry.

have plotted the phonon density of states of the repeated slab with the ideally terminated surface geometry (dashed curve) and with the asymmetric relaxed surface geometry (solid curve). The peaks S_2 at around 30 meV and S_3 at around 42 meV are due to localized surface states in the stomach gaps. The peak S_2 is not observed for the unrelaxed surface geometry, that is, it clearly arises due to the formation of surface dimers, as do peaks S_4 and S_5. On the other hand, the peak S_3 *can* be seen with the unrelaxed surface geometry, although it is not in the gap region for this geometry.

(ii) Polarization and localization of surface modes. In this section we will present discussion on polarization and localization of surface-phonon modes for which vibrational amplitudes are largest for the first and second layer atoms. Due to 3° of freedom per atom and a total of four atoms per surface unit cell, we have 12 surface vibrational modes for a chosen phonon wave vector, with the lowest three being acoustic. In the following discussion, diagrams of displacement patterns have been provided for those phonon modes whose eigenvectors have negligible imaginary components. Where the imaginary components are non-negligible, the polarization characteristics have been described, but it is not possible to display displacement patterns graphically for such cases. In selected cases we also list the parity of phonon modes relative to the mirror plane containing the dimer.

(a) At the $\bar{\Gamma}$ *point*. In Table II, we present our calculated surface-phonon modes on Si(001)(2×1). We also present the displacement patterns of 12 surface phonon modes at the $\bar{\Gamma}$ point in Fig. 7. The lowest three nonzero surface frequencies at 5.42, 5.43, and 7.72 meV are acoustic modes with all atoms in the top two surface layers moving in phase. The lowest frequency 5.42 meV results from the vibrations of the first layer and second layer atoms in the dimer row direction, [110]. The second nonzero surface frequency at 5.43 meV is due to the motion of the atoms in the top two layers in the dimer bond direction, [110]. The third nonzero surface frequency at 7.72 meV is due to vibrations of the top two layer atoms perpendicular to the surface.

These lowest three phonon modes are actually Lamb waves[41] (i.e. plate modes, rather than true surface modes). The lowest energy pair are antisymmetric ''flexural'' modes, while the other is symmetric. At the zone center, only three such modes are expected. Lamb wave frequencies are dependent upon the thickness of the slab, and tend towards that of the Rayleigh wave as the slab thickness tends to infinity. This may be clearly seen in Fig. 8, which shows the zone center Lamb wave frequencies dropping towards zero as the slab thickness is increased in test calculations. All phonon frequencies presented in this paper, other than these three, are well-converged with respect to the slab thickness, since they are not Lamb waves.

The phonon mode at 14.86 meV has a complex character with vibrations from the top two layer atoms. The phonon mode at 25.49 meV is a dimer rocking mode with opposing vibrations of the first layer atoms. This phonon mode has been reported at 21.2 meV in a recent *ab initio* calculation.[15] The phonon mode at 32.89 meV is characterized by parallel motion of the first layer atoms, while the second layer atoms vibrate perpendicular to each other. The phonon mode at 48.50 meV is due to opposing vibrations of the first and second layer atoms. The phonon mode at 58.05 meV comes from the vibrations of the second layer atoms perpendicular to each other while the first layer atoms vibrate in the dimer row direction. The phonon mode at 61.32 meV is characterized by opposing vibrations of the top two layer atoms in the dimer row direction. Finally, we have observed the highest surface optical frequency at the $\bar{\Gamma}$ point at 69.25 meV. For this phonon mode, the first layer atoms vibrate against each other while the second layer atoms vibrate perpendicular to each other.

We have estimated the Rayleigh wave (RW) velocity close to the $\bar{\Gamma}$ point by averaging the velocities in both the $\bar{\Gamma}$-J and $\bar{\Gamma}$-J' directions. The RW velocity was found to be $V_{\mathrm{RW}}=4930\ \mathrm{ms}^{-1}$, in good agreement with the experimental value of $V_{\mathrm{RW}}^{\mathrm{exp}}=5020\ \mathrm{ms}^{-1}$ measured by Dutcher *et al.* using Brillouin light scattering,[25] and the value of $V_{\mathrm{RW}}=4860\ \mathrm{ms}^{-1}$ calculated by Fritsch and Pavone.[15]

TABLE II. Calculated surface-phonon frequencies of Si(001)(2×1) at the $\bar{\Gamma}$ point and their comparison with a recent *ab initio* calculation. The symmetry is defined with respect to the mirror plane perpendicular to the dimer rows (+ is even, − is odd). Frequencies are given in meV.

Reference	Modes at $\bar{\Gamma}$											
Present results	5.42	5.43	7.72	14.86	17.28	25.49	32.89	37.74	48.50	58.05	61.32	69.25
Symmetry	−	+	+	+	−	+	+	+	+	−	−	+
(Reference 15)						21.2						63.6
Symmetry						+						+

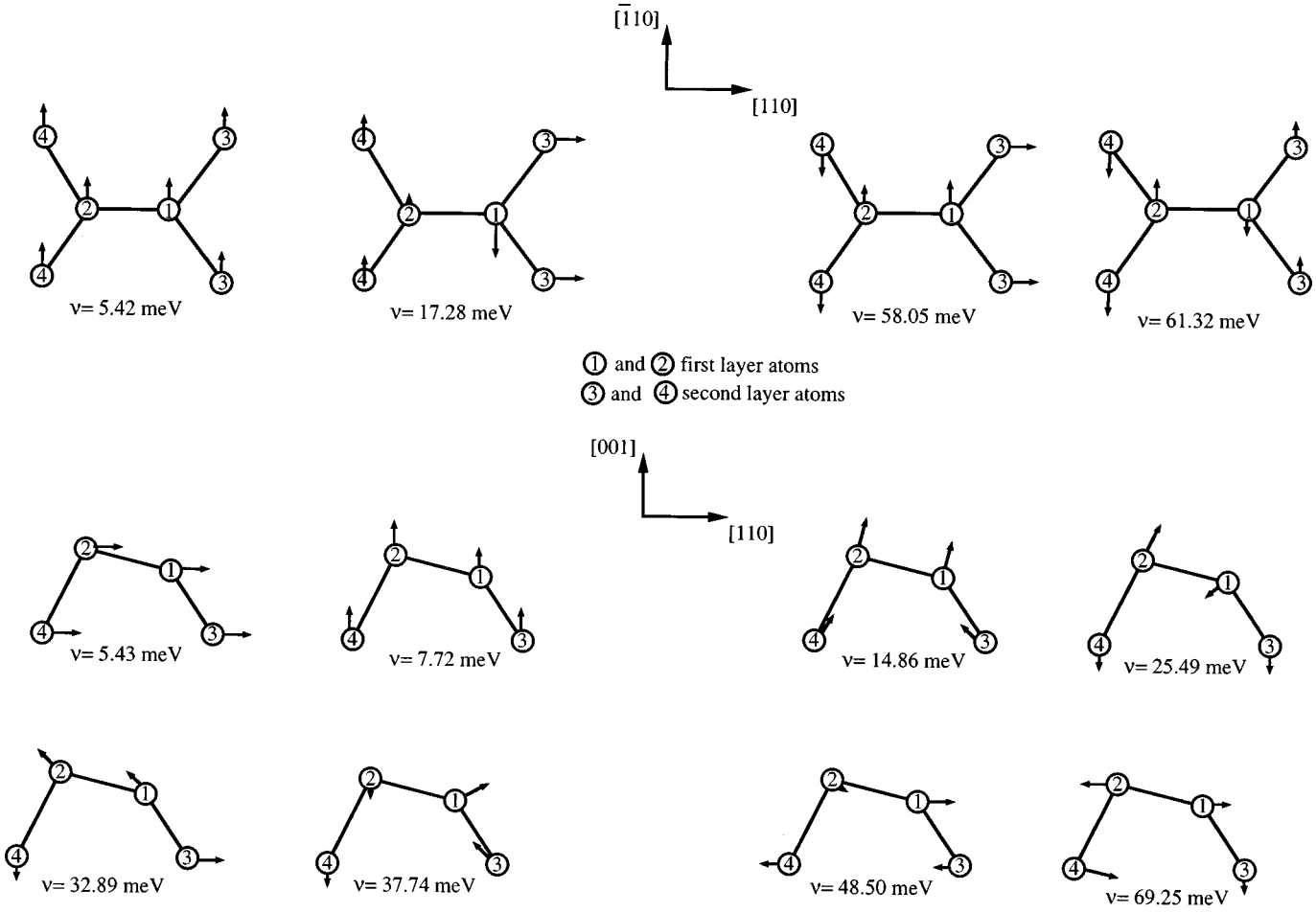

FIG. 7. Atomic displacement patterns of twelve surface-phonon modes at the $\overline{\Gamma}$ point.

(b) At the $\overline{J'}$ point. Away from the $\overline{\Gamma}$ point, it is convenient to describe phonon modes as having either sagittal plane (SP) or shear horizontal (SH) polarization. The sagittal plane is defined as that plane containing both the two-dimensional phonon wave vector and the surface normal vector, while shear horizontal vibrations are those which occur perpendicular to the sagittal plane. In Table III, we present calculated surface- phonon frequencies and their polarization characters (calculated including contributions from all 16 layers in the slab) for some modes on Si(001) $\times(2\times1)$ at the $\overline{J'}$ point. We also compare our results with earlier theoretical calculations.[27,29,30,15]

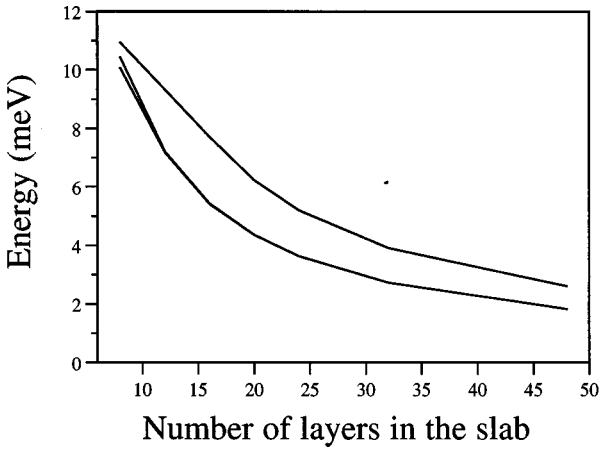

FIG. 8. Variation of zone center Lamb wave frequencies with slab thickness.

The RW phonon mode at 13.60 meV is totally polarized as SP with parallel vibrations of the first layer atoms in the surface normal direction. A similar displacement pattern for this phonon mode has also been found by Fritsch and Pavone[15,42] with a much lower energy. In other words, while in our work we find the RW in resonance with the bulk spectrum, the work of Fritsch and Pavone characterizes it as a true surface mode below the bulk continuum. On the other hand, the energy of our RW mode at $\overline{J'}$ agrees well with two earlier tight-binding calculations by Alerhand and Mele,[29] and by Mazur and Pollmann.[30]

The phonon mode at 14.98 meV has a displacement pattern similar to the RW mode. The phonon mode at 15.55 meV is mainly due to the second layer atoms vibrating in phase along the surface normal. Fritsch and Pavone also obtained a phonon mode at 12.53 meV with a similar displacement pattern. The phonon mode at 18.05 meV is 80% SP polarized and corresponds to vibrations of the first layer atoms with components in both the surface normal and dimer bond directions, while second layer atoms vibrate in the dimer row direction. The phonon mode at 21.56 meV agrees with the phonon mode at 20.63 meV in the theoretical work of Fritsch and Pavone[42] with respect to its energy location and polarization behavior. For this phonon mode, the first

TABLE III. Comparison of calculated surface phonons on Si(001)(2×1) at the $\overline{J'}$ point with results of earlier theoretical calculations. Also tabulated are normalized summations of the ionic displacements in the shear horizontal plane (SH) and the sagittal plane (SP), including contributions from all layers in the supercell. Frequencies are given in meV.

Reference	Modes at $\overline{J'}$											
Present results	13.60	14.98	15.55	18.05	21.56	27.63	29.83	38.10	45.94	51.66	53.12	65.12
$[\Sigma U^2_{SP}]$	1.00	0.91	0.88	0.78	0.37	0.83	0.78	0.92	0.56	0.77	0.80	0.28
$[\Sigma U^2_{SH}]$	0.00	0.09	0.12	0.22	0.63	0.17	0.22	0.08	0.44	0.23	0.20	0.72
Reference 27												~68.7
Reference 29	13.6											61.1
Reference 30	~13.7											~64.0
Reference 15	9.24		12.53		20.63							

layer atoms vibrate against each other in the surface normal direction while they move parallel to each other in the dimer bond direction.

The phonon mode at 29.83 meV is a true localized surface-phonon mode with 80% SP polarization. The phonon mode at 38.1 meV corresponds to the motion of the first layer atoms in the dimer row direction while the second layer atoms vibrate with components both in the surface normal and dimer bond directions. The phonon mode at 45.94 meV comes from the motion of the second layer atoms in the dimer bond direction while the first layer atoms vibrate in both the dimer bond and surface normal directions. The phonon mode at 51.66 meV has 77% SP character with vibrations of the second layer atoms in the dimer bond direction. The highest surface optical mode at 65.12 meV has 72% SH character and mainly corresponds to the vibrations of second layer atoms with components in both the surface normal and dimer bond directions.

(c) At the K point. Some of the phonon frequencies and their comparison with earlier theoretical calculations[27,29,30,15] at $\overline{K}$ are listed in Table IV. Note that the Rayleigh wave only becomes a true surface localized state along $\overline{J}$-$\overline{K}$ and close to $\overline{K}$ along $\overline{K}$-$\overline{J'}$. The RW frequency of 15.77 meV at the $\overline{K}$ point corresponds to the vibrations of the first layer atoms with components in both the surface normal and dimer bond directions, while the second layer atoms move in the dimer row direction. A similar displacement pattern for this phonon mode also has been observed by Fritsch and Pavone.[42] However, they have obtained a significantly lower frequency of 10.30 meV for the RW. On the other hand, our calculated energy for this phonon mode is in agreement with earlier tight-binding calculation results.[29,30]

The phonon mode at 18.88 meV at $\overline{K}$ results from the vibrations of the first and second layer atoms in the dimer row and surface normal directions, respectively. The phonon mode at 20.92 meV is a rocking phonon mode with opposing vibrations of the first layer atoms. This phonon mode has been reported at 20.0 meV in the work of Fritsch and Pavone,[15,42] respectively.

The phonon modes at 29.40 meV, 43.20 meV, 45.73 meV, and 53.97 meV are localized stomach gap phonon modes and their displacement patterns are shown in Fig. 9. The phonon mode at 29.40 meV comes from opposing vibrations of first layer atoms in the dimer row direction while the second layer atoms move in the dimer bond direction. Fritsch and Pavone[15,42] have observed a phonon mode at 35.2 meV in the stomach gap region also with large displacements from the first layer atoms in the dimer row direction. The phonon mode at 43.20 meV is a swinging mode with vibrations of the first layer atoms in the dimer row direction. This phonon mode can be compared to the phonon modes at 44.2 meV and 41.1 meV in the works of Allan and Mele[26] and Fritsch and Pavone,[15] respectively.

We have observed a dimer stretching phonon mode at 45.77 meV which has been reported at 42.7 meV by Fritsch and Pavone.[15] The phonon mode at 61.64 meV corresponds to opposing vibrations of the first layer atoms in the dimer bond direction. The highest surface optical frequency is due

TABLE IV. Calculated surface-phonon frequencies of Si(001)(2×1) at the $\overline{K}$ point and their comparison with earlier theoretical calculations. Also tabulated are normalized summations of the ionic displacements in the shear horizontal plane (SH) and the sagittal plane (SP), including contributions from all layers in the supercell. Frequencies are given in meV.

Reference	Modes at $\overline{K}$								
Present results	15.77	18.88	20.92	29.40	43.2	45.77	53.97	61.64	65.48
$[\Sigma U^2_{SP}]$	0.70	0.87	0.73	0.48	0.67	0.61	0.80	0.45	0.34
$[\Sigma U^2_{SH}]$	0.30	0.13	0.27	0.52	0.33	0.39	0.20	0.55	0.66
Reference 27									~68.0
Reference 29	14.4								61.2
Reference 30	~14.5								~63.2
Reference 15	10.3		20.0	~35.2	41.1	42.7			59.3

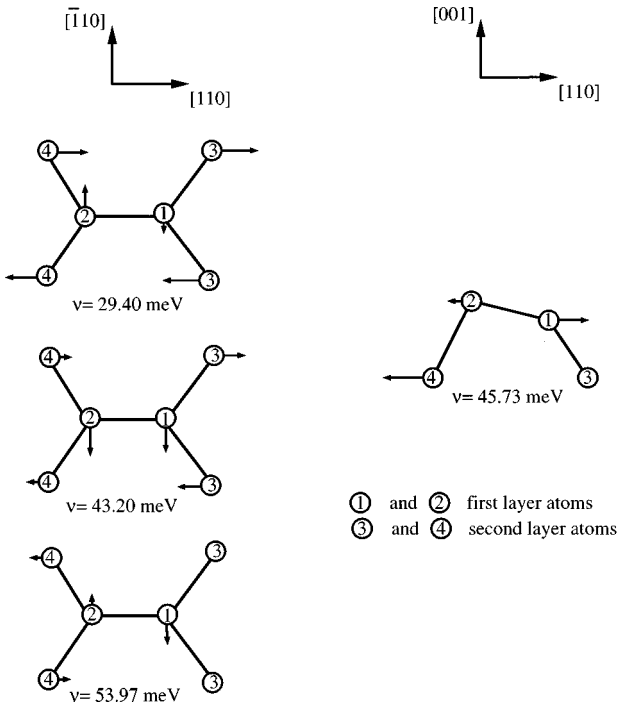

FIG. 9. Atomic displacement patterns of localized gap phonon modes at the $\bar{K}$ point.

to the vibrations of the second layer atoms with components both in the surface normal and dimer bond directions while the first layer atoms vibrate in the dimer row direction. Allan and Mele[26] also observed large vibrational amplitudes from the second layer atoms for this phonon mode [see Fig. 3(c) in Ref. 26].

(d) At the $\bar{J}$ point. Some of the phonon energies and their comparison with earlier theoretical calculations[27,29,30,15] at the $\bar{J}$ point are given in Table V. The Rayleigh phonon mode at 8.38 meV is purely sagittal and mainly corresponds to the vibrations of the first layer atoms with components both in the surface normal and dimer bond directions. The phonon mode of 10.30 meV is characterized by the vibrations of the first and second layer atoms with components both in the surface normal and dimer bond directions. The phonon mode at 16.24 meV is purely shear horizontal and results from vibrations of the top three layer atoms in the dimer row direction.

The phonon mode at 22.37 meV has been placed at 22.6 meV in the work of Fritsch and Pavone[15] and is a rocking phonon mode with the vibrations of the first layer atoms in both the surface normal and dimer bond directions. The phonon mode at 50.14 meV is totally SP polarized and mainly corresponds to the opposing motion of the second layer atoms in the surface normal direction. The phonon mode at 58.75 meV is due to the opposing vibrations of the first and second layer atoms in the dimer row direction. The phonon mode at 62.13 meV is totally SP with vibrations of the top two layer atoms in both the surface normal and dimer bond direction. The highest surface-phonon mode at 69.45 meV is due to vibrations of the first and second layer atoms with components in both the surface normal and dimer bond directions. Finally, comparing the displacement patterns of the highest surface optical phonon mode at the symmetry points, we find that the atomic displacement patterns corresponding to the highest surface optical phonon mode are wave vector dependent (i.e., are different at different points on the surface Brillouin zone).

IV. SUMMARY

In this paper, we have presented a study of the phonon modes for the symmetric and asymmetric dimer models of the Si(001)(2×1) surface calculated within the phenomenological adiabatic bond-charge model. The atomic geometry and dangling bond charges are taken from an *ab initio* pseudopotential calculation. In general, our results are in agreement with earlier theoretical calculations. For relaxed symmetric and asymmetric dimer models we find that the tilt of the dimer results in the energy of zone-edge surface phonons dropping by up to 2 meV, with the consequence that the Rayleigh mode (the lowest surface-phonon mode) becomes more distinct from the bulk phonon modes for the tilted dimer. In particular, we have obtained the energy of the Rayleigh frequency at $\bar{K}$ in agreement with tight-binding calculations, whereas a recent *ab initio* calculation by Fritsch and Pavone obtained a significantly lower energy for this mode.

Comparison of our results for relaxed and unrelaxed geometries reveals that dimerization leads to new peaks in the phonon density of states. In particular, the stomach gap peak at around 30 meV is a strong signature of dimer formation,

TABLE V. Comparison of calculated surface phonons on Si(001)(2×1) at the $\bar{J}$ point with results of earlier theoretical calculations. Also tabulated are normalized summations of the ionic displacements in the shear horizontal plane (SH) and the sagittal plane (SP), including contributions from all layers in the supercell. Frequencies are given in meV.

Reference	Modes at $\bar{J}$							
Present results	8.39	10.30	16.24	22.37	50.14	58.75	62.13	69.45
$[\Sigma U^2_{SP}]$	1.00	1.00	0.00	1.00	1.00	0.00	1.00	1.00
$[\Sigma U^2_{SH}]$	0.00	0.00	1.00	0.00	0.00	1.00	0.00	0.00
Reference 27								~70.3
Reference 29	~8.0							~64.6
Reference 30	~8.8							~65.0
Reference 15	9.0			22.6				~63.9

since no stomach gap phonon modes are obtained for the unrelaxed surface geometry. We have also presented a discussion on the location and polarization characteristics of some surface-phonon modes at the symmetry points. It is also found that the atomic displacement pattern corresponding to the highest surface optical mode is wave vector dependent.

Our results clearly indicate that the adiabatic bond-charge model, utilizing a relaxed atomic geometry obtained from *ab initio* pseudopotential calculations, is a reliable theoretical technique for the study of surface phonons on Si(001)(2 $\times$1). Future work will concentrate on the vibrational properties of the $c(4\times2)$ reconstruction of the (001) surface, and of overlayers on the (001) surface.

ACKNOWLEDGMENTS

H.M.T. gratefully acknowledges financial support by the University of Sakarya in Turkey. S.J.J. would like to acknowledge the financial support of the EPSRC (UK). The computational work has been supported by the EPSRC (UK) through the CSI scheme.

[1] J. C. Fernandez, W. S. Ying, H. D. Shih, F. Jona, D. Jepsen, and P. M. Marcus, J. Phys. C **14**, L55 (1981).
[2] W. S. Yang, F. Jona, and P. M. Marcus, Solid State Commun. **43**, 847 (1982).
[3] B. W. Holland, C. B. Duke, and A. Paton, Surf. Sci. **140**, L269 (1984).
[4] G. Jayaram, P. Xu, and L. D. Marks, Phys. Rev. Lett. **71**, 3489 (1993).
[5] R. Rossmann, H. L. Meyerheim, V. Jahns, J. Wever, W. Moritz, D. Wolf, D. Dornich, and H. Schulz, Surf. Sci. **279**, 199 (1992).
[6] E. Fontes, J. R. Patel, and F. Comin, Phys. Rev. Lett. **70**, 2790 (1993).
[7] C. A. Lucas, C. S. Dower, D. F. McMorrow, G. C. L Wong, F. J. Lamelas, and P. H. Fuoss, Phys. Rev. B **47**, 10 375 (1993).
[8] W. R. Lambert, P. L. Trevor, M. J. Cardillo, A. Sakai, and D. R. Hamann, Phys. Rev. B **35**, 8055 (1987).
[9] R. I. G. Uhrberg, G. V. Hansson, J. M. Nicholls, and S. A. Flodström, Phys. Rev. B **24**, 4684 (1981).
[10] L. S. O. Johansson, R. I. G. Uhrberg, P. Martensson, and G. V. Hansson, Phys. Rev. B **42**, 1305 (1990).
[11] M. C. Payne, N. Roberts, R. J. Needs, M. Needels, and J. D. Joannopoulos, Surf. Sci. **211/212**, 1 (1989).
[12] I. P. Batra, Phys. Rev. B **41**, 5048 (1990).
[13] E. Artacho and F. Yndurain, in *Physics of Semiconductors: Proceedings of the 20th International Conference*, edited by E. M. Anastassakis and J. D. Joannopoulos (World Scientific, Singapore, 1990), p. 167.
[14] P. Krüger and J. Pollmann, Phys. Rev. Lett. **74**, 1155 (1995).
[15] J. Fritsch and P. Pavone, Surf. Sci. **344**, 159 (1995).
[16] S. J. Jenkins and G. P. Srivastava, J. Phys. Condens. Matter **8**, 6641 (1996).
[17] D. Badt, H. Wengelnik, and H Neddermeyer, J. Vac. Sci. Technol. B **12**, 2015 (1994).
[18] A. I. Shkrebtii, R. Difelice, C. M. Bertoni, and R. Del Sole, Phys. Rev. B **51**, 11 201 (1995).
[19] A. Ramstad, G. Brocks, and P. J. Kelly, Phys. Rev. B **51**, 14 504 (1995).
[20] J. Northrup, Phys. Rev. B **47**, 10 032 (1993).
[21] U. Harten and J. P. Toennies, Europhys. Lett. **4**, 833 (1987).
[22] M. B. Nardelli, D. Cvetko, V. De Renzi, L. Floreano, A. Morgante, M. Peloi, and F. Tommasini, Phys. Rev. B **52**, 16720 (1995).
[23] H. Nienhaus and W. Mönch, Phys. Rev. B **50**, 11 750 (1994).
[24] H. Nienhaus and W. Mönch, Surf. Sci. **328**, L561 (1995).
[25] J. R. Dutcher, S. Lee, B. Hillebrands, G. J. McLaughlin, B. G. Nickel, and G. I. Stegeman, Phys. Rev. Lett. **68**, 2464 (1992).
[26] D. C. Allan and E. J. Mele, Phys. Rev. Lett. **53**, 826 (1984).
[27] J. Pollmanm, R. Kalla, P. Krüger, A. Mazur, and G. Wolfgarten, Appl. Phys. A **41**, 21 (1986).
[28] A. Mazur and J. Pollmann, Phys. Rev. Lett. **57**, 1811 (1986).
[29] O. L. Alerhand and E. J. Mele, Phys. Rev. B **35**, 5533 (1987).
[30] A. Mazur and J. Pollmann, Surf. Sci. **255**, 72 (1990).
[31] W. Weber, Phys. Rev. Lett. **33**, 371 (1974).
[32] K. C. Rustagi and W. Weber, Solid State Commun. **18**, 673 (1979).
[33] H. M. Tütüncü and G. P. Srivastava, J. Phys. Condens. Matter **8**, 1345 (1996).
[34] H. M. Tütüncü and G. P. Srivastava, Phys. Rev. B **53**, 15 675 (1996).
[35] L. Miglio, P. Ruggerone, and G. Benedek, Phys. Scr. **37**, 768 (1988)
[36] U. Harten, J. P. Toennies, C. Woll, L. Miglio, P. Ruggerone, L. Colombo, and G. Benedek, Phys. Rev. B **38**, 3305 (1988).
[37] G. B. Bachelet, D. R. Hamann, and M. Schlüter, Phys. Rev. B **26**, 4199 (1982).
[38] A. A. Maradudin, E. W. Montroll, G. H. Weiss, and I. P. Ipatova, *Theory of Lattice Dynamics in the Harmonic Approximation*, 2nd ed. (Academic, New York, 1971).
[39] P. N. Keating, Phys. Rev. **145**, 637 (1966).
[40] W. Mönch, *Semiconductor Surfaces and Interfaces*, 2nd ed. (Springer, Berlin, 1995), p. 159.
[41] I. A. Viktorov, *Rayleigh and Lamb Waves* (Plenum Press, New York, 1967), Chap. 2.
[42] J. Fritsch and P. Pavone (private communication).